bioRxiv preprint doi: https://doi.org/10.1101/2023.12.07.565988; this version posted December 8, 2023. The copyright holder for this preprint (which was not certified by peer review) is the author/funder, who has granted bioRxiv a license to display the preprint in perpetuity. It is made available under aCC-BY-ND 4.0 International license.

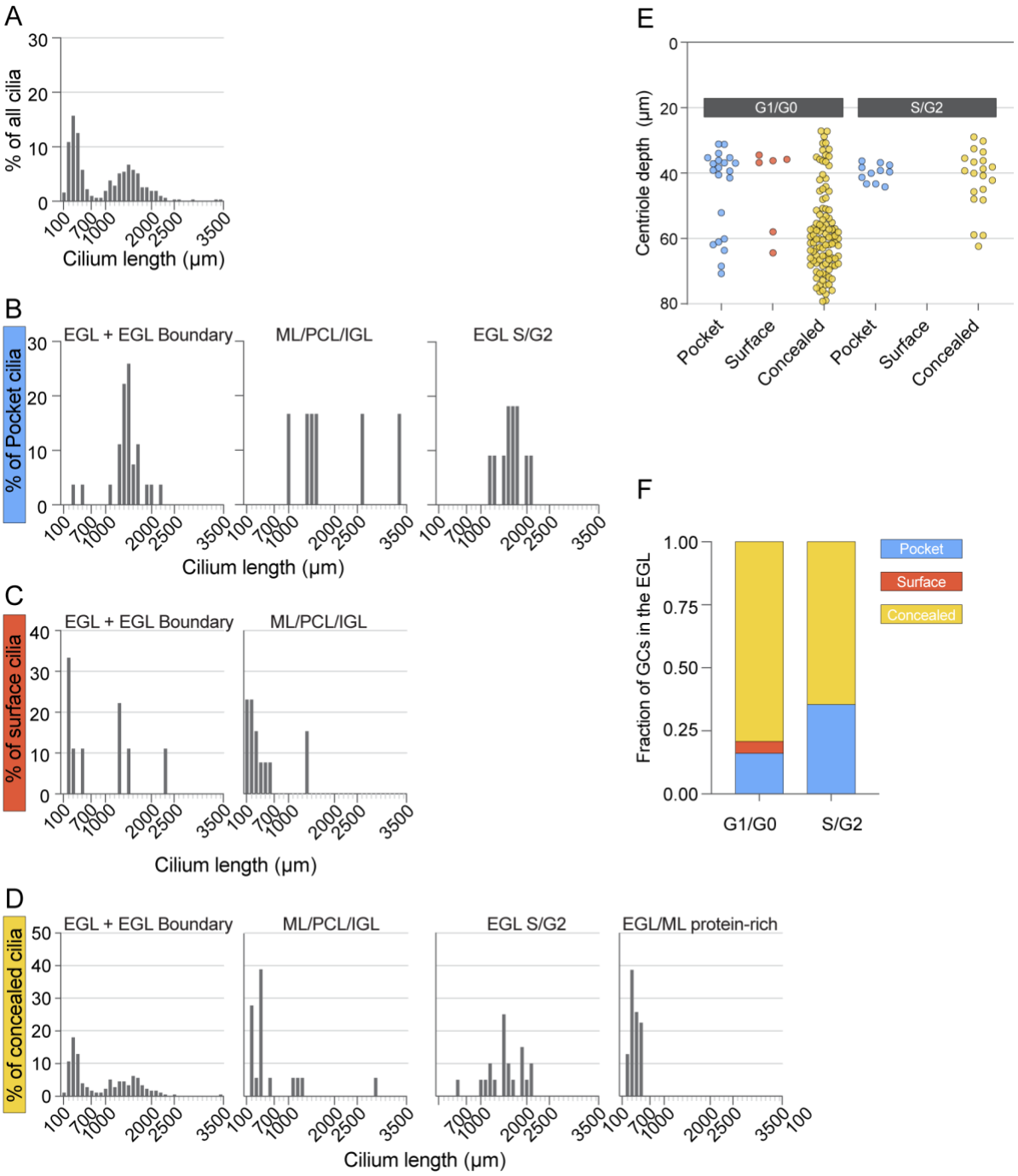

Supplemental Figure 1. Bimodal distribution of cilia lengths.
(A) Cilia from the P7 volume were binned by 100 nm and the distribution of cilia lengths was plotted as a percentile of total cilia.
(B-D) The distribution of cilia lengths plotted in A is separated by pocket (B), surface (C), and concealed (D) cilia types. Within each cilium type the distributions are shown by cell layer with S/G2 cilia and protein-rich cilia plotted separately. There are no s/G2 cells with surface cilia and all protein-rich cilia are concealed.

bioRxiv preprint doi: https://doi.org/10.1101/2023.12.07.565988; this version posted December 8, 2023. The copyright holder for this preprint (which was not certified by peer review) is the author/funder, who has granted bioRxiv a license to display the preprint in perpetuity. It is made available under aCC-BY-ND 4.0 International license.

(E) The depth of the basal body for each cilium in the EGL is plotted based on cilium type. Cells in G1/G0 are on the left and cells in S/G2 are on the right.
(F) The pocket, surface and concealed cilia in the EGL are plotted as a fraction of the total G1/G0 cells and S/G2 cells. Cells in the EGL boundary were excluded from E and F.

bioRxiv preprint doi: https://doi.org/10.1101/2023.12.07.565988; this version posted December 8, 2023. The copyright holder for this preprint (which was not certified by peer review) is the author/funder, who has granted bioRxiv a license to display the preprint in perpetuity. It is made available under aCC-BY-ND 4.0 International license.

A

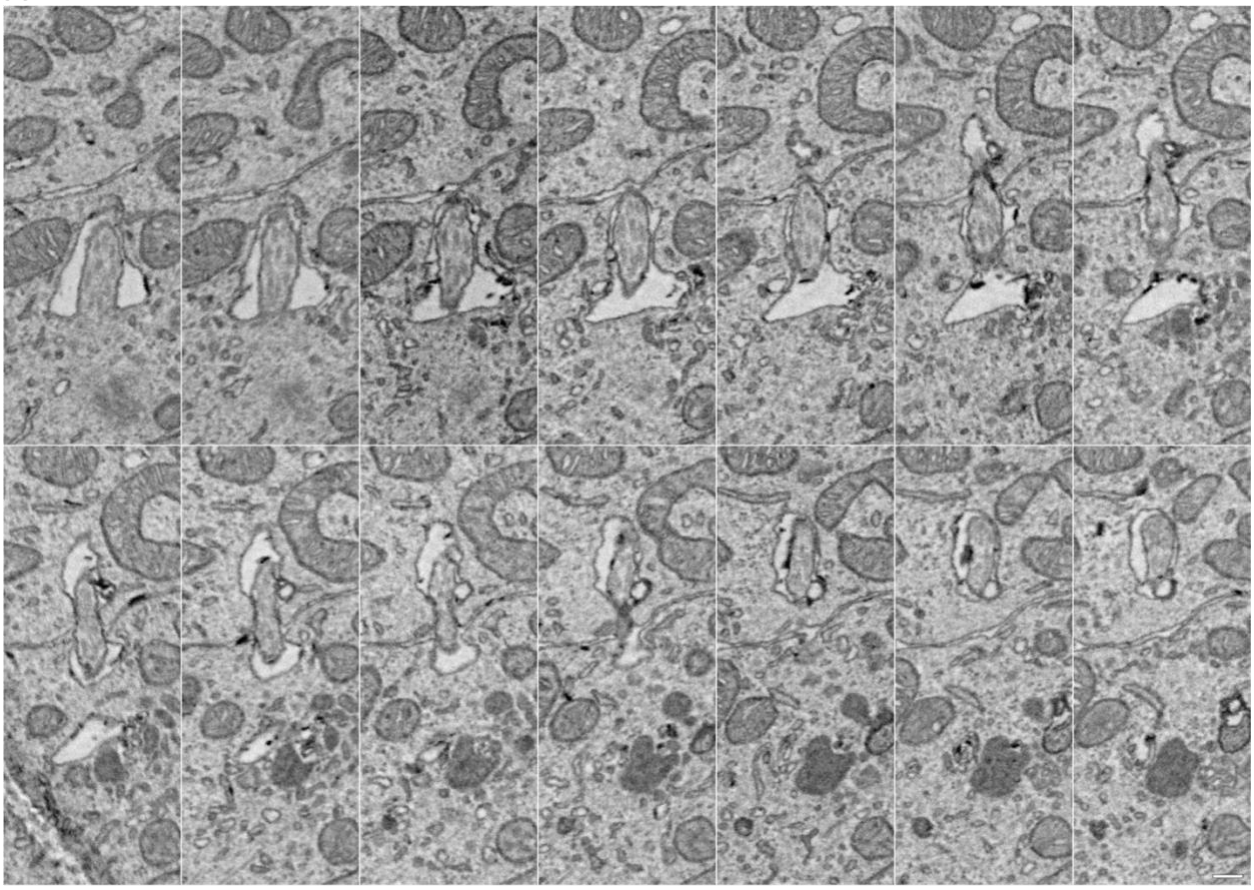

B

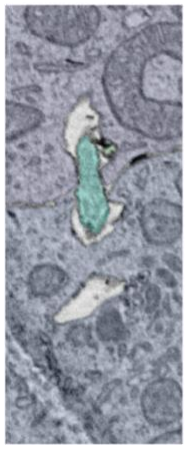

C

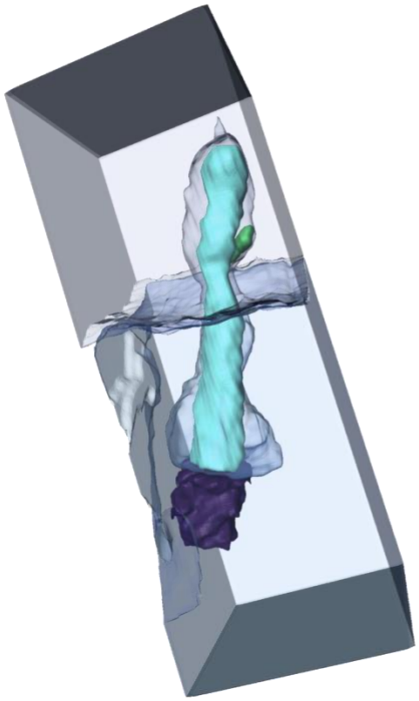

bioRxiv preprint doi: https://doi.org/10.1101/2023.12.07.565988; this version posted December 8, 2023. The copyright holder for this preprint (which was not certified by peer review) is the author/funder, who has granted bioRxiv a license to display the preprint in perpetuity. It is made available under aCC-BY-ND 4.0 International license.

Supplemental Figure 2. Cilium enveloped by an adjacent cell.
(A) Serial EM sections of a pocket cilium that exits the cell in the bottom half of the image and is enveloped by the adjacent cell. Scale bar is 200 nm and z interval is 30 nm.
(B) Single z slice from the sections in A colored to highlight the cilium (cyan), the cell of cilium origin (blue) and the enveloping cell (lavender).
(C) 3D reconstruction of the same cilium. The basal body is purple and the membrane inclusion adjacent to the cilium is green.

bioRxiv preprint doi: https://doi.org/10.1101/2023.12.07.565988; this version posted December 8, 2023. The copyright holder for this preprint (which was not certified by peer review) is the author/funder, who has granted bioRxiv a license to display the preprint in perpetuity. It is made available under aCC-BY-ND 4.0 International license.

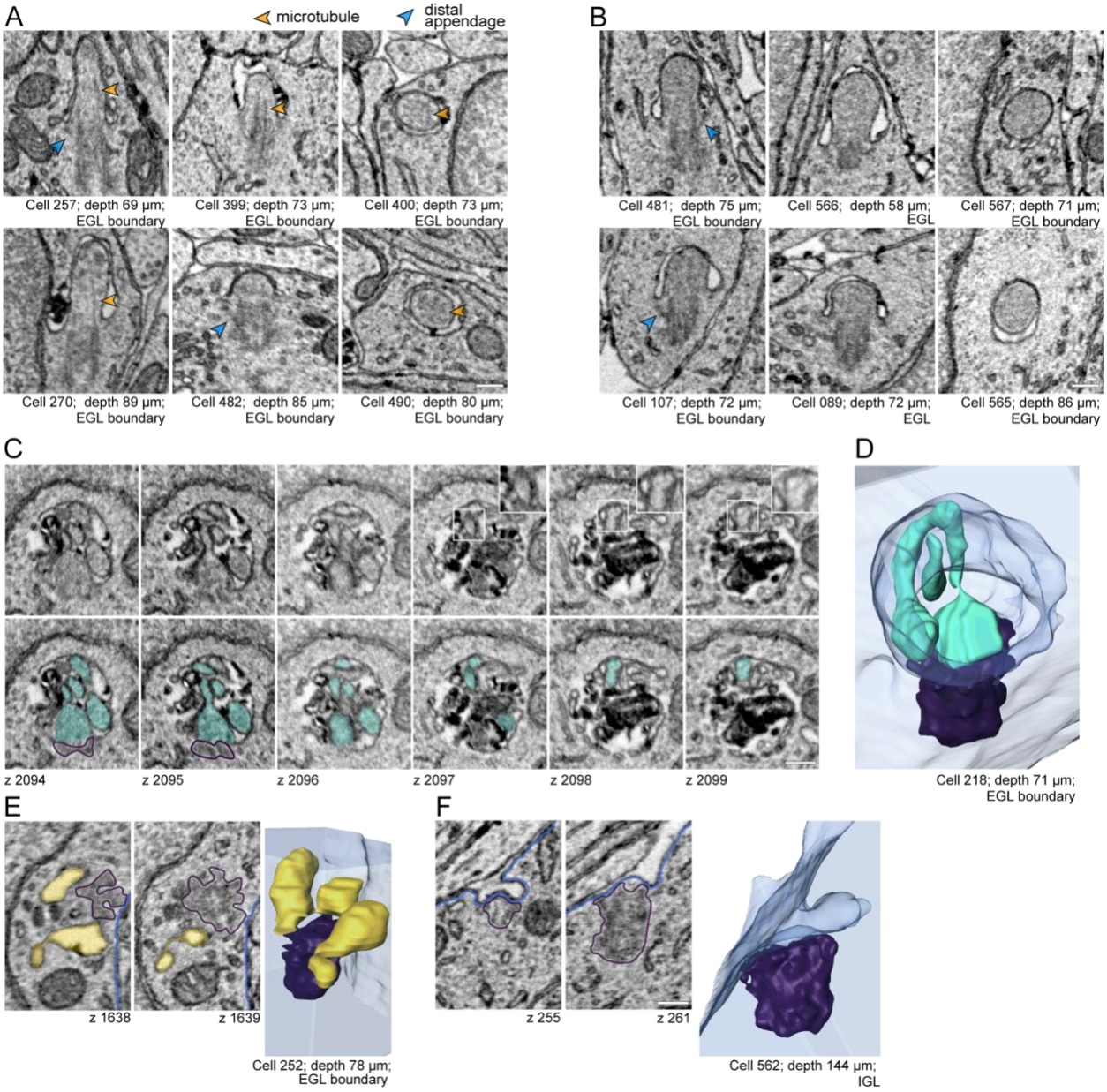

Supplemental Figure 3. Cilium deconstruction and docking intermediates.
(A-B) Representative images of short cilia with electron lucent (A) or electron rich (B) cilioplasm. Microtubules are highlighted with orange arrowheads and distal appendages with blue arrowheads. The scale bar is 200 nm.
(C-D) A single cilium was observed with a constriction that could be indicative of cilium severing. Serial EM sections are shown in C. Microtubule singlets are visible in the insets on the top row and the cilium (and potential cilium fragment) are shaded cyan in the lower panel. A view of the 3D segmented image is presented in D.
(E) A mother centriole in the EGL boundary that has three vesicles each docked at a different subset of distal appendages.
(F) A centriole in the IGL with a membrane invagination anchored at distal appendages. Scale bars are 200 nm.

bioRxiv preprint doi: https://doi.org/10.1101/2023.12.07.565988; this version posted December 8, 2023. The copyright holder for this preprint (which was not certified by peer review) is the author/funder, who has granted bioRxiv a license to display the preprint in perpetuity. It is made available under aCC-BY-ND 4.0 International license.

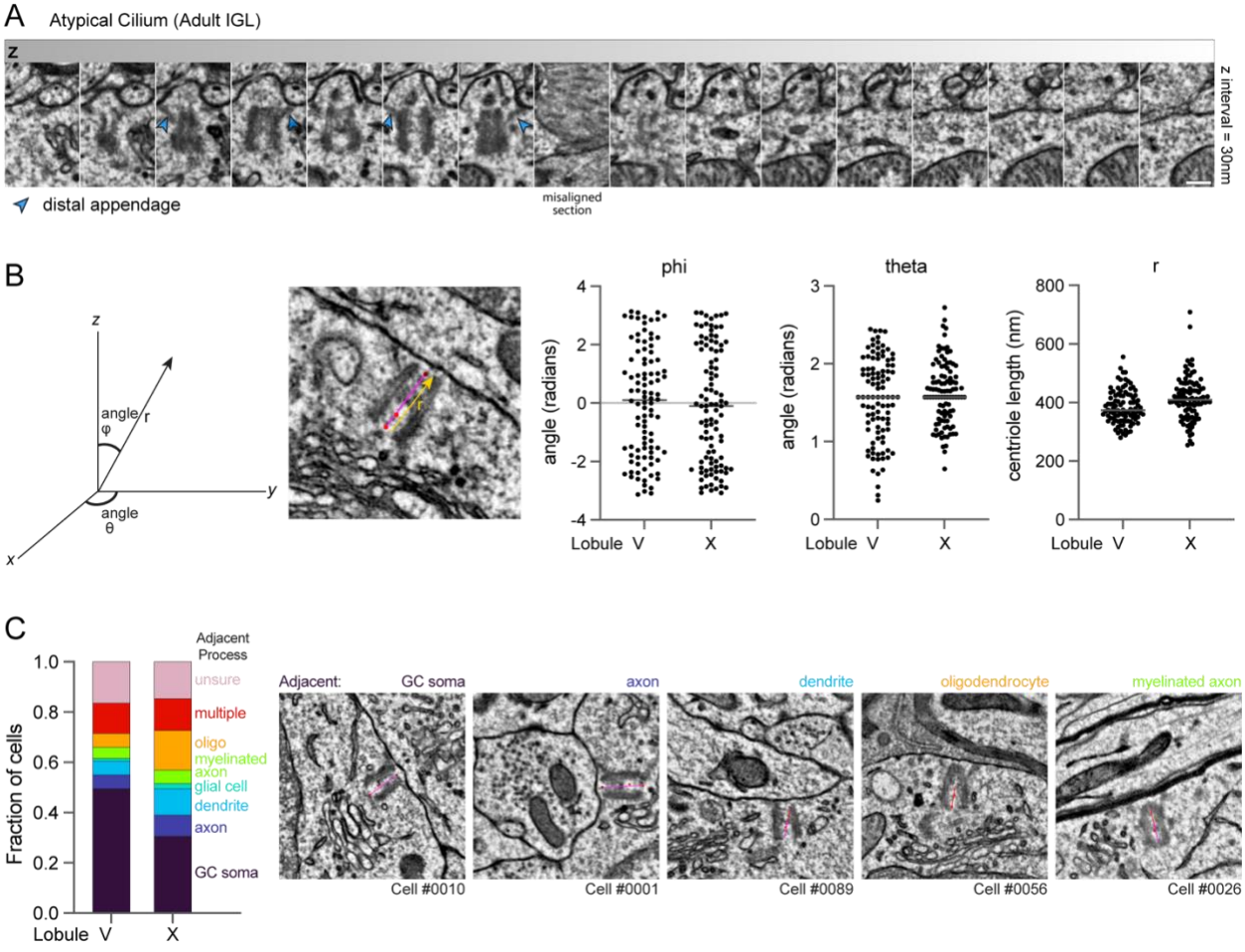

Supplemental Figure 4. Docked centrioles in adult GCs lack directed orientation.
(A) Serial EM sections display the only cilium annotated in the adult IGL volumes. Internal vesicles are present and the axoneme is not present or not resolved. Scale bar is 200 nm.
(B) To assess polarity of centriole docking we generated a vector from proximal to distal within each mother centriole. We compared the vectors and found no bias in the orientation of docked centrioles.
(C) The type of structure immediately adjacent to the plasma membrane where each GC mother centriole docked was determined. The distributions for the annotated centrioles in each adult dataset are plotted on the left and EM images on the right provide examples of centrioles docked adjacent to the indicated structures.

bioRxiv preprint doi: https://doi.org/10.1101/2023.12.07.565988; this version posted December 8, 2023. The copyright holder for this preprint (which was not certified by peer review) is the author/funder, who has granted bioRxiv a license to display the preprint in perpetuity. It is made available under aCC-BY-ND 4.0 International license.

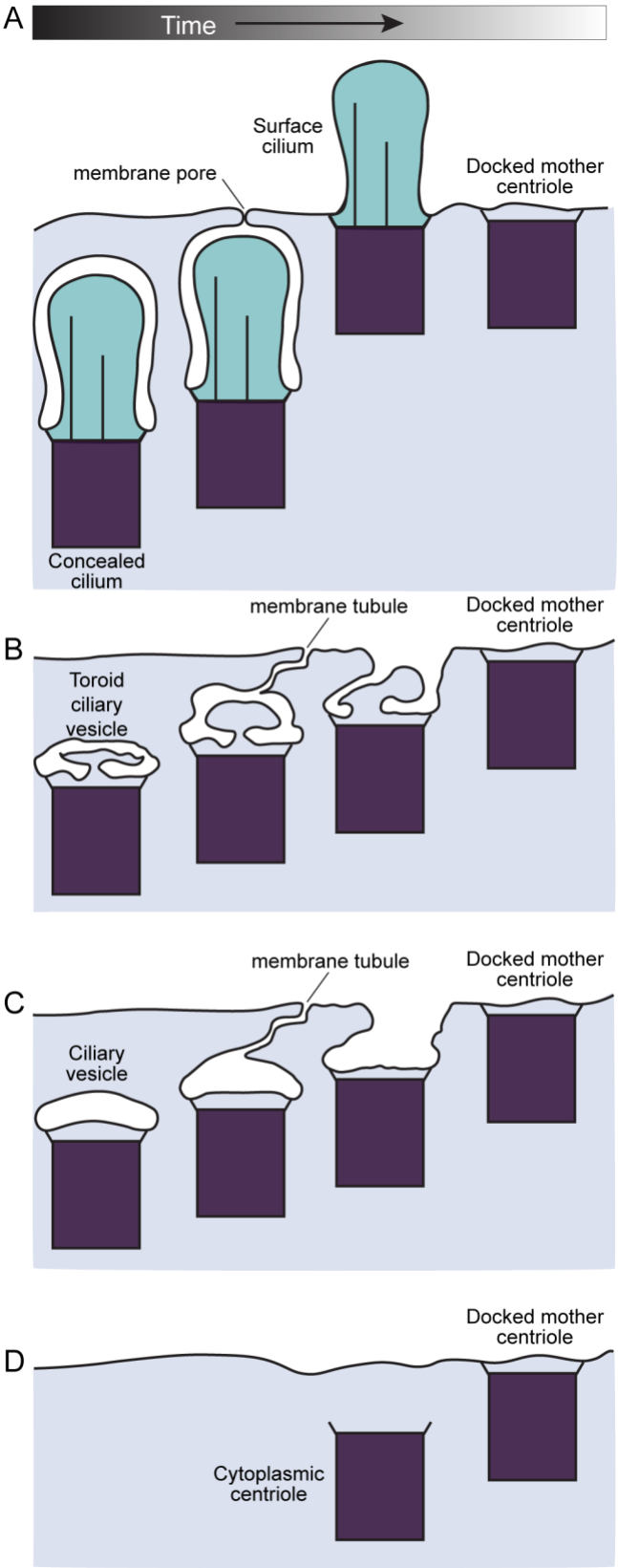

bioRxiv preprint doi: https://doi.org/10.1101/2023.12.07.565988; this version posted December 8, 2023. The copyright holder for this preprint (which was not certified by peer review) is the author/funder, who has granted bioRxiv a license to display the preprint in perpetuity. It is made available under aCC-BY-ND 4.0 International license.

Supplemental Figure 5. Centriole docking initiated at different stages in cilia deconstruction could account for the variety of intermediates observed.

Differences between late-stage cilia/centrosome structures in differentiating cells suggest that instead of a linear deconstruction pathway, variance in the coordination of cilia deconstruction and mother centriole docking could generate multiple routes to mature, unciliated cells with docked mother centrioles.

(A) Concealed cilia could access the plasma membrane through observed membrane pores. Opening of the pore before the cilium has been deconstructed could result in surface cilia, which could subsequently be completely disassembled.

(B and C) Cilia deconstruction could proceed such that ciliary vesicles remain while centriole docking commences. Dynamic tubules could be key to unite the ciliary vesicle with the plasma membrane.

(D) Conventional plasma membrane docking of cytoplasmic mother centrioles, which have completely deconstructed cilia, could proceed similar to centriole docking during surface cilia biogenesis and at the immune synapse.